Enhanced magnetic hybridization of a spinterface through insertion of a two-dimensional magnetic oxide layer

Alberto Brambilla,[*,†] Andrea Picone,[†] Dario Giannotti,[†] Giulia Berti,[†,‖]
Gianlorenzo Bussetti,[†] Simona Achilli,[‡] Guido Fratesi,[‡] Mario I. Trioni,[¶]
Giovanni Vinai,[§] Piero Torelli,[§] Giancarlo Panaccione,[§] Lamberto Duò,[†] Marco
Finazzi,[†] and Franco Ciccacci[†]

*Dipartimento di Fisica, Politecnico di Milano, piazza Leonardo da Vinci, 32 - 20133
Milano, Italy, Dipartimento di Fisica, Università degli Studi di Milano, Via Celoria, 16,
Milano, Italy, CNR National Research Council of Italy, ISTM, via Golgi 19, Milan, Italy,
and Laboratorio TASC, IOM-CNR, S.S. 14 km 163.5, Basovizza, I-34149 Trieste, Italy*

E-mail: alberto.brambilla@polimi.it

Abstract

Interfaces between organic semiconductors and ferromagnetic metals offer intriguing opportunities in the rapidly developing field of organic spintronics. Understanding and controlling the spin-polarized electronic states at the interface is the key towards

---

*To whom correspondence should be addressed
†Dipartimento di Fisica, Politecnico di Milano, piazza Leonardo da Vinci, 32 - 20133 Milano, Italy
‡Dipartimento di Fisica, Università degli Studi di Milano, Via Celoria, 16, Milano, Italy
¶CNR National Research Council of Italy, ISTM, via Golgi 19, Milan, Italy
§Laboratorio TASC, IOM-CNR, S.S. 14 km 163.5, Basovizza, I-34149 Trieste, Italy
‖Present address: Department of Chemical Physics, Fritz-Haber-Institut der Max-Planck-Gesellschaft, Faradayweg 4-6, 14195 Berlin, Germany

a reliable exploitation of this kind of systems. Here we propose a novel approach to achieve such goals, namely the insertion of a two-dimensional magnetic oxide layer at the interface, with the aim of both increasing the reproducibility of the interface preparation and offering a way for a further fine control over the electronic and magnetic properties. We have inserted a two-dimensional Cr_4O_5 layer at the C_{60}/Fe(001) interface and we have characterized the corresponding morphological, electronic and magnetic properties. Scanning tunneling microscopy and electron diffraction show that the film grows well ordered both in the monolayer and multilayer regimes. Electron spectroscopies confirm that hybridization of the electronic states occurs at the interface. Finally, magnetic dichroism in x-ray absorption leads to the observation of an unprecedented spin-polarization of the hybridized fullerene states, thus confirming the efficacy of the new approach.

In the last decade, organic semiconductors (OS) have demonstrated to be promising candidates for advanced spintronics applications.[1–4] In particular, they show long spin lifetimes and, despite the low carrier mobility, also conducting paths of the order of 100 nm.[3,5] C_{60} fullerene is a prototypical OS for organic spintronics, as it shows ideal properties like a good energy level matching with ferromagnetic (FM) metallic thin films, the presence of a low hyperfine interaction (giving long spin lifetimes), the possibility of being sublimated in ultra-high vacuum (UHV) and the robustness necessary to be integrated in layered magnetic structures.[6–8] As a matter of fact, significant room temperature magnetoresistance has already been observed for spin valves based on C_{60}.[5,7,9–12]

Several studies have clearly shown that the mechanisms governing performances such as the effective injection of spins into organic layers, are strongly dependent on the detailed properties of the OS/FM interface, called spinterface, which can be determined by, for instance, hybridization of the electronic states,[13,14] insertion of a polar layer,[15,16] interface resistance,[17] crystal structure.[18] In particular, the formation of hybridized interface states has been demonstrated to have a direct influence on the spin polarization of the current injected at the interface.[19–21] Such an effect is mostly evident when the spin character of the

2

injected current is reversed with respect to the polarization of the FM electrode.[13]

The above considerations support the conclusion that the control over the chemical re-actions occurring at the interface are a way through which one can achieve the desired spin-polarized characteristics of the spinterface. It is therefore important that such reactions can be mastered and reliably reproduced during sample preparations, which is not easy when dealing with reactive surfaces like those of FM metals.[22] One way to overcome such issues is that of inserting a relatively thick oxide layer between FM and OS,[23] which is more notably effective at the upper layer of an on organic spin valve, where the rough morphology of an OS layer may lead to undesired effects like the formation of pinholes.[10] In the present work we propose a different approach, which consists in inserting a ultra-thin oxide (in the limit of two-dimensional layer) at the spinterface. Such an approach aims to offer a further mean of tailoring both the electronic, magnetic and structural properties of the interface and, also, to increase the reproducibility of such properties. From the latter viewpoint, in fact, an oxidized surface is potentially less exposed to changes in preparation conditions when subsequently growing the OS layer.

We used C_{60} as OS and Fe(001) as FM materials, and we considered different possible preparations of the Fe surface, subsequently resulting in different interfaces. The C_{60}/Fe(001) case has already been explored, from the point of view of interface hybridization, by de Jong and coworkers.[8,24] Recently, we have been able to study and compare the early stages of formation of C_{60} fullerene layers on the clean Fe(001) surface and the oxygen-passivated Fe(001)-$p(1 \times 1)$O surface.[25] The comparison between the two different systems have high-lighted the role that oxygen plays in determining the coupling between the OS and the metal. In fact, dramatic differences were observed both from the point of view of surface morphol-ogy, as the molecule diffusivity was substantially enhanced by the presence of oxygen, and electronic properties, being characterized by a lower hybridization (thus by an effective de-coupling) again in the Fe(001)-$p(1 \times 1)$O case. Such differences are expected to influence also the magnetic properties of the hybridized molecular states.

3

Here, we employ X-ray Magnetic Circular Dichroism (XMCD) to investigate the magnetic hybridization of the fullerene interface states, due to the interaction with the underlying FM surface, in both C_{60}/Fe(001) and C_{60}/Fe(001)-$p(1 \times 1)$O. We furthermore move to the new approach by inserting a Cr_4O_5 monolayer (ML) at the C_{60}/Fe interface. Such a two-dimensional Cr oxide has been demonstrated to form a stable wetting layer on Fe(001), characterized by a regular array of Cr vacancies which results in a $(\sqrt{5} \times \sqrt{5})R26.6°$ surface symmetry.[26] This system shows also a long-range FM order with a magnetization oriented in-plane and anti-parallel with respect to that of the underlying Fe.[27] We indeed observe a spin-polarization of the hybridized C_{60} states in all cases, and a significant enhancement of the magnetic effects at the C_{60}/Cr_4O_5/Fe(001) interface, which confirms the efficacy of the new design.

The magnetic investigations are supported by several other measurements, which are described first, in order to have a wide comparison of the role of the differently prepared interfaces in driving the formation of the hybridized interface states. We employ Scanning Tunneling Microscopy (STM) to investigate how C_{60} grows onto the Cr oxide surface. The electronic interactions at the interface are evaluated by means of Photoemission Spectroscopy (PES) and Inverse Photoemission Spectroscopy (IPES); experimental details about the latter techniques are given in Ref. 28. In all cases, the sample preparation steps are the same as discussed in previous publications.[25,26,29,30] The results are eventually discussed and supported also in terms of an ab-initio theoretical analysis.

All STM measurements reported hereafter were realized at room temperature (RT), in UHV conditions, with an Omicron VT-STM microscope and homemade W tips. We previously reported, in Ref. 25, STM topography images revealing that C_{60} molecules on both Fe(001) and Fe(001)-$p(1 \times 1)$O have quite low diffusion rates in the very early stages of growth (fraction of a molecular layer). Fig. 1a) shows the same low coverage case for C_{60}/Cr_4O_5/Fe(001). The situation appears to be markedly different, as fullerene molecules are observed to either stick to the edges of the substrate's islands or to form clusters, thus
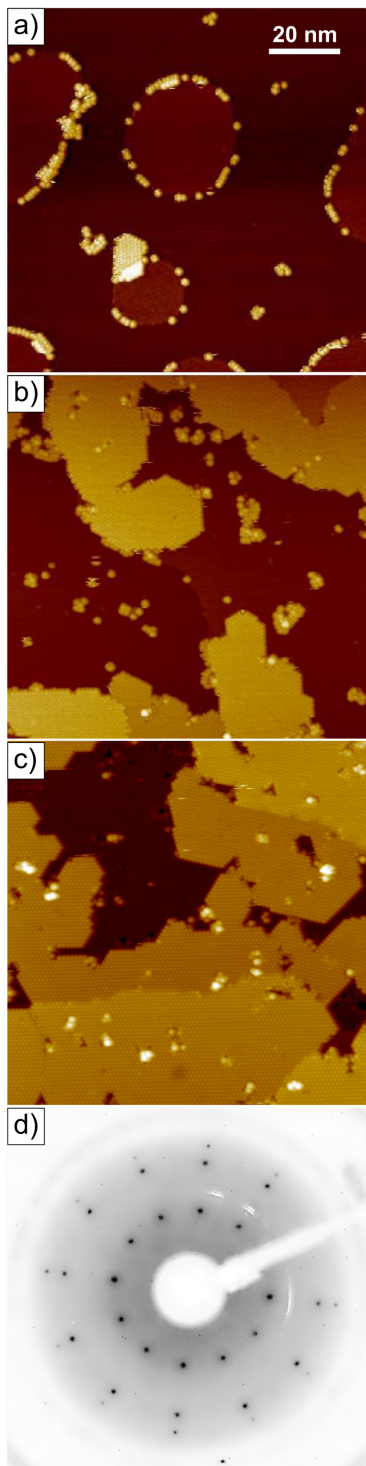
Figure 1: a-c) Scanning tunneling microscopy images illustrating the early stages of growth of C_{60} over the Cr_4O_5/Fe(001) surface. The nominal fullerene coverage is: a) 0.1 ML (tunneling parameters $\Delta V = 1.5$ V, $I = 500$ pA); b) 0.5 ML ($\Delta V = 1.7$ V, $I = 400$ pA); c) 1.2 ML ($\Delta V = 1.5$ V, $I = 400$ pA). Each image size is about 100×100 nm^2. d) Low energy electron diffraction pattern recorded for a thick (about 3 ML) C_{60} film on Cr_4O_5/Fe(001). The electron beam energy is 22 eV.

5

indicating a greater surface diffusivity. When increasing the coverage in the sub-monolayer regime, the Fe(001) and Fe(001)-$p(1 \times 1)$O cases start to differentiate, being the former still characterized by a very low diffusivity, without island formation, and the latter featuring both well-separated molecules and C_{60} islands at the same time.[25] The higher diffusivity observed for $C_{60}/Cr_4O_5/Fe(001)$ in the very early stages of growth characterizes also this second regime. In fact, Fig. 1b) shows a very low number of isolated molecules, while larger ML-thick islands are present. This increased diffusivity reflects in a well-ordered growth at higher thicknesses, as testified in Fig. 1c) for a coverage above 1 ML and from the Low-Energy Electron Diffraction (LEED) pattern, which is related to a multilayer fullerene film (about 3 ML thick). The LEED pattern is characterized by sharp spots and a negligible background. The diffraction spots are disposed in a way that reflects the hexagonal close-packed arrangement typical of compact C_{60} films, featuring rings of 12 spots that correspond to equivalent domains rotated by 90°, on account of the fourfold symmetry of the substrate.
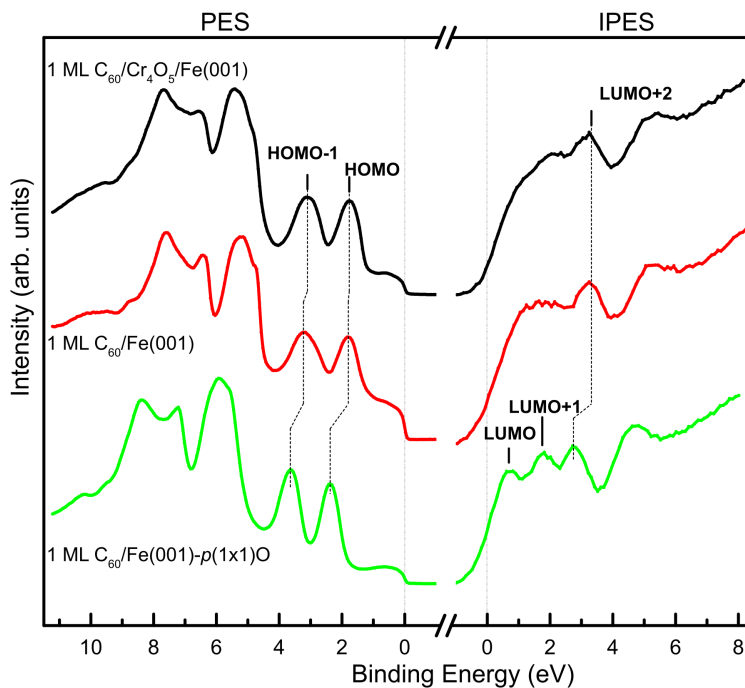

Figure 2: Photoemission (left, $h\nu = 21.2$ eV) and inverse photoemission (right, $h\nu = 9.4$ eV, isochromatic mode) spectra acquired on 1 ML C_{60} grown onto $Cr_4O_5/Fe(001)$ (black dots, upper spectrum), clean Fe(001) (red dots, middle spectrum) and Fe(001)-$p(1 \times 1)$O (green dots, lower spectrum).

The different behavior in terms of molecular diffusion on the surface might be associated to a different charge transfer between C_{60} and the various substrates. Fig. 2 compares the PES/IPES spectra, taken in the -10 eV to 8 eV binding energy range, for a C_{60} monolayer on Cr_4O_5/Fe(001) (black spectra, top row), Fe (001) (red spectra, middle row) and Fe(001)-$p(1 \times 1)$O (green spectra, bottom row), where the last two spectra were already discussed in Ref. 25 and are shown here for comparison. We remark that the Fe(001)-$p(1 \times 1)$O spectra can be considered to be representative of a C_{60} fullerene film, as the interaction with the substrate is substantially negligible,[25] and the lineshapes are in very good agreement with previous measurements.[31,32] The PES/IPES spectra for 1 ML C_{60}/Cr_4O_5/Fe(001) are very similar to those reported for 1 ML C_{60}/Fe(001), both in terms of line shape and peak positions, which differ by less than 100 meV for the HOMO-1 and HOMO peaks and are equal for the LUMO+2 peak. In both 1 ML C_{60}/Cr_4O_5/Fe(001) and 1 ML C_{60}/Fe(001) the LUMO and LUMO+1 peaks are merged and, thus, indistinguishable. The latter feature can be understood in terms of a significant electronic coupling at the interface.

In order to unveil the relationship between the electronic coupling and the magnetic properties of the spinterfaces, we performed XMCD measurements at the C K_1 edge. The latter were taken at the APE-HE beamline of the Elettra synchrotron.[33] The XAS spectra were acquired in the total electron yield mode, with the photon beam impinging at 45° with respect to the sample surface. The samples were oriented so to have one of the easy axes of magnetization of the Fe(001) surface in the same plane containing both the radiation propagation vector and the normal to the sample surface, in order to maximize the spin-polarized signal. All spectra were acquired at RT and in the remanent magnetization condition, after applying a magnetic field pulse of 50 Oe, which is largely enough to saturate the substrates magnetization. Fig. 3 presents both XAS spectra at opposite x-ray circular polarizations and the relative XMCD spectra, for 1 ML C_{60} grown on the different surfaces considered in this work, plus a multilayer C_{60}/Cr_4O_5/Fe(001) case (about 2 ML C_{60} thickness). The XAS spectra are characterized by the typical C_{60} lineshape, where the C $1s \rightarrow \pi^*$ absorption peaks
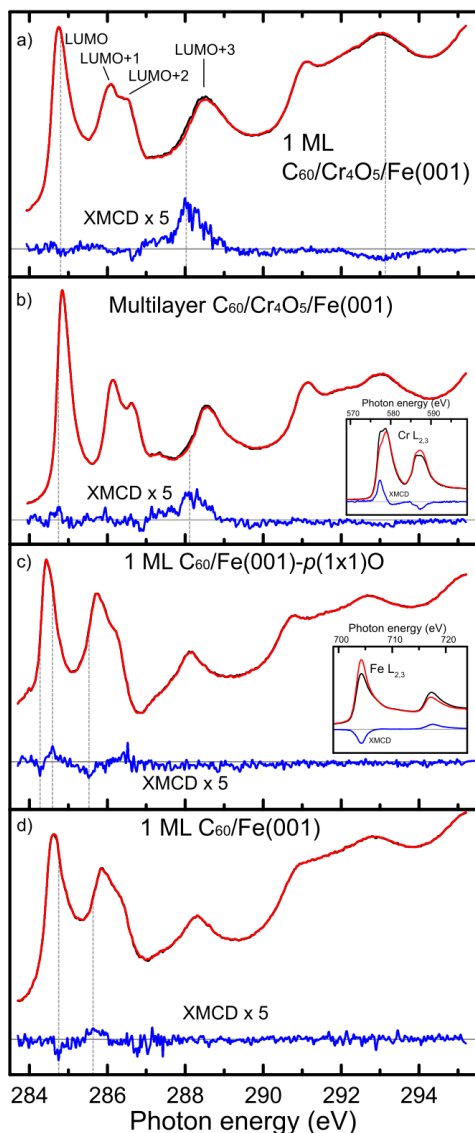
Figure 3: X-ray absorption spectroscopy at the C K_1 edge performed with either right (black lines) or left (red lines) circular polarization and corresponding XMCD spectra (blue lines) of, from bottom to top: 1 ML C_{60}/Fe(001), 1 ML C_{60}/Fe(001)-$p(1 \times 1)$O, a multilayer (about 2 ML) C_{60}film on Cr_4O_5/Fe(001), 1 ML C_{60}/Cr_4O_5/Fe(001). The XMCD spectra are multiplied by 5, as indicated. The vertical dashed lines indicate the peaks in the XMCD spectra. Inset of b): XAS and XMCD spectra of 1 ML C_{60}/Cr_4O_5/Fe(001) at the Cr $L_{2,3}$ edge. Inset of c): XAS and XMCD spectra of 1 ML C_{60}/Fe(001) at the Fe $L_{2,3}$ edge.

are labeled increasingly from LUMO to LUMO+3. The part of the spectra above about 289 eV (C_{60} ionization potential) are instead due to C $1s \rightarrow \sigma^*$ transitions. The LUMO+1 and LUMO+2 peaks are merged together in the $C_{60}/Fe(001)$ case (Fig. 3d), on account of the stronger interaction with the substrate, as already observed in several cases where fullerene was grown on metallic substrates.[34–36] In the $C_{60}/Cr_4O_5/Fe(001)$ samples (Figs. 3a and 3b) and, to some extent, also in the $C_{60}/Fe(001)$-$p(1 \times 1)O$ case, the LUMO+1 and LUMO+2 peaks are better resolved, more similarly to the C_{60}/Fe_3O_4 case.[37] The LUMO peak positions, summarized in Table 1, reflect the trend already observed for the IPES peaks reported in Fig. 2.

Table 1: Summary of energy positions for LUMO and XMCD peaks reported in Fig. 3. The last column reports the ratio between each XMCD peak intensity and the corresponding average XAS intensity (see text).

Sample	LUMO peak (eV)	XMCD peak (eV)	XMCD/XAS (%)
1 ML $C_{60}/Cr_4O_5/Fe(001)$	284.75	284.80	-1.26
		288.00	11.98
		293.00	-1.52
Multil. $C_{60}/Cr_4O_5/Fe(001)$	284.85	284.77	1.93
		288.10	9.84
1 ML $C_{60}/Fe(001)$-$p(1 \times 1)O$	284.40	284.27	-5.26
		284.60	2.97
		285.50	-4.36
1 ML $C_{60}/Fe(001)$	284.60	284.75	-3.80
		285.65	1.97

From the point of view of the magnetic hybridizations of the fullerene molecules at the interface, we observe first of all that in all cases reported in Fig. 3 the measured XMCD is different from zero at correspondence with different absorption peaks, revealing that a spin-polarization has been induced in the C_{60} π-conjugated states. The main peaks observed in the XMCD spectra of Fig. 3 are summarized in Table 1, in terms of their energy position and of the ratio between the XMCD peak intensity and the corresponding average XAS intensity (at the same photon energy position). It must be underlined that the order with which the XAS spectra at different polarizations are subtracted to obtain the XMCD spectrum is the

same that produces a corresponding XMCD spectrum of the Fe substrate at the Fe $L_{2,3}$ edge characterized by a negative first XMCD peak (see inset of Fig. 3c): this way the sign of all the XMCD spectra at the C K_1 edge can be reliably compared. Notice that the corresponding XMCD spectrum of Cr_4O_5 at the Cr $L_{2,3}$ edge (see inset of Fig. 3b) is positive, on account of the anti-parallel coupling with the underlying Fe.[27] All XMCD spectra are rescaled by a factor of about 1.5 that takes into account the fact that the X-ray beam impinges at 45° on the sample surface and that the actual degree of circular polarization is about 95%. The spectra are further multiplied by a factor 5, as indicated in Fig. 3, in order to make the peaks more visible. The latter factor is not included in the data of Table 1.

Concerning the pristine C_{60}/Fe(001) interface, our XMCD spectrum shows many similarities with that obtained in Ref. 36. In particular, we also observe an oscillatory behavior with XMCD changing sign when passing from the LUMO to the LUMO+1/+2 positions. The maximum relative intensity of the XMCD (of about 3.8% of the XAS signal) is also in good agreement with the previous results. Minor differences are represented by the slightly different energy positions of the peaks and by the absence of a sizeable dichroic signal for the C $1s \rightarrow \sigma^*$ part of the spectrum. Coming to the C_{60}/Fe(001)-$p(1 \times 1)$O interface, despite the apparently lower interaction with the substrate suggested by the photoemission spectra, we observe again an oscillatory coupling with a maximum XMCD value now increased to above 5% of the XAS signal. Such an increase might be due to the enhanced spin-polarization of the Fe(001)-$p(1 \times 1)$O surface states with respect to those of Fe(001), as well known from both experiments and theory.[29,38,39] Finally, both monolayer and multilayer cases are reported in Figs. 3a) and 3b), respectively, for the C_{60}/Cr_4O_5/Fe(001) system. The XMCD spectra are dominated by a large positive signal at about 288.0 eV, close to the LUMO+3 peak. As reported in Table 1, this XMCD peak reaches a value of nearly 12% for the monolayer case, which is unprecedented in similar (purely carbon-based) systems, where a maximum value of only about 5% has been reported for the hybridized π^* states of graphene on Ni(111).[40] Differently from the other cases, here we also observe an XMCD peak, of opposite sign,

in the σ^* states of C_{60}, while minor oscillations of the XMCD signal are seen close to the LUMO and LUMO+2 peaks. The consistency of the observation is further confirmed by the spectra related to the multilayer (about 2 ML) $C_{60}/Cr_4O_5/Fe(001)$, where the attenuation of the signal due to the increased coverage leaves visible only the largest peak, here centered at 288.1 eV, which is now reduced to less than 10% of the corresponding XAS signal. This is fully consistent with the interface nature of the hybridized C_{60} states.

In order to understand the striking results obtained when inserting Cr_4O_5 at the $C_{60}/Fe(001)$ interface, we have performed a theoretical analysis based on first-principle density functional theory (DFT) simulations, with the generalized gradient approximation to account for the exchange and correlation functionals, as proposed by Perdew, Burke, and Ernzerhof (GGA-PBE),[41] taking into account the spin polarization in a collinear description. A deep characterization of the interface morphology is a formidable task and it is out of the scope of the present work. Accordingly, we have chosen here a representative configuration to describe the molecule-substrate interaction. We consider a $c(2 \times 2)$ supercell and placed the C_{60} molecules in a squared arrangement with the pentagon on top of a Cr vacancy. According to the literature,[24] the molecules-surface distance was set equal to 2 Å and the C_{60} was not relaxed. We adopt the surface geometry reported in Ref. 26 for the $(\sqrt{5} \times \sqrt{5})R26.6°$ reconstruction, obtained by leaving the two topmost Fe layers and the Cr_4O_5 atoms free to relax. A vacuum region of 12 Å separates repeated slabs from each other. The plane-wave ultrasoft pseudopotential method[42] was used as implemented in the PWSCF code of the Quantum-ESPRESSO distribution.[43] Pseudopotentials were generated starting from scalar-relativistic all-electron atomic calculations and using non-linear core corrections. Semicore $3s3p$ states are included for Cr. In order to describe the XMCD spectra of carbon, for which one electron is promoted from the $1s$ core state to the Fermi level, we describe one of the C atoms in the pentagon in front of the surface by using the half core hole approximation, as discussed in Ref. 44, i.e. by appropriately building the pseudopotential with half filling of the core state. Kinetic energy cutoffs are 55 Ry for the wavefunctions and 280 Ry for the effective potential

and the charge density. The surface Brillouin zone sampling has been performed with the Monkhorst-Pack[45] scheme, adopting integration meshes equivalent to at least a 14×14 mesh in the irreducible surface unit cell of Fe(001).
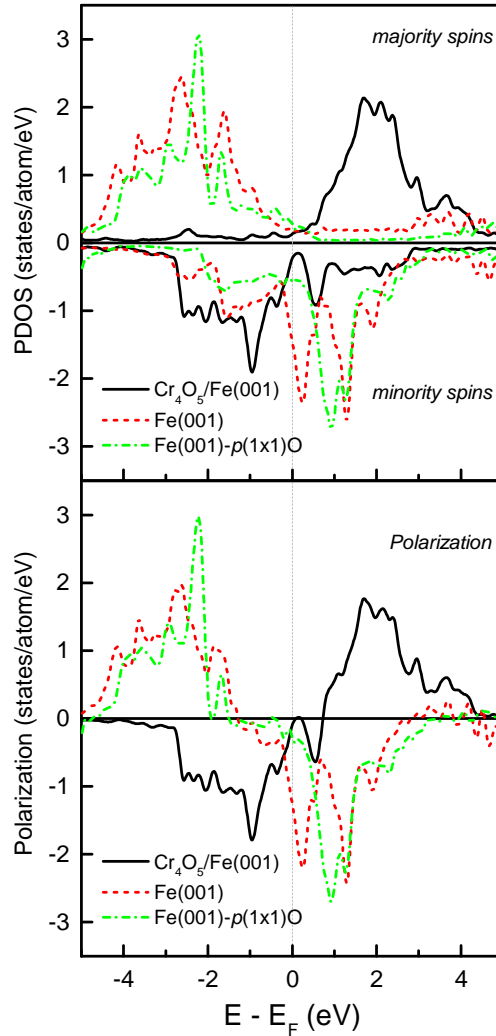

Figure 4: Projected density of states and spin polarization of Fe(100), Fe(001)-$p(1 \times 1)$O and $(\sqrt{5} \times \sqrt{5})R26.6°$/Fe(100) surfaces.

A qualitative explanation of the differences in XMCD spectra of C_{60} on different surfaces can be inferred by the magnetic properties of the substrate electronic states. The spin polarization of the molecule is indeed reasonably due to the hybridization with the d-states of the underlying surface. Fig. 4 displays the majority and minority spin Projected Density of States (PDOS) relative to the $3d$ atom in the outermost surface layer (top panel) and the

spin polarization (bottom panel) for the three surfaces considered, namely Fe(100), Fe(001)-$p(1 \times 1)$O and Cr_4O_5/Fe(001). The clean and oxidized Fe surfaces display states located in similar energy ranges, apart for a small shift toward higher energies that characterizes minority spin states of the Fe(001)-$p(1 \times 1)$O substrate, leading to an increase of the total magnetization. Differently, the Cr PDOS is characterized by opposite spin polarization, accordingly to the AF ordering of Cr atoms with respect to the underlying Fe atoms.[26,27] Furthermore, the center of the d band of Cr is shifted by about 1.5 eV with respect to that of the clean Fe(100) surface. The unoccupied C_{60} molecular levels are expected to hybridize with the available states just above the Fermi level E_F. For C_{60} on Fe(001) and Fe(001)-$p(1 \times 1)$O, the molecular orbitals can interact with the minority spin states, while in Cr_4O_5 the hybridization can occur with the large majority spin peak at higher energy (~ 2 eV). These differences in the PDOS of the three surfaces are consistent with the different energy positions of the features observed in the XMCD spectra.

It is worth noting that, when a C_{60} molecule is adsorbed on the Cr_4O_5 surface, a description of the magnetic character of the interface becomes more difficult for the core excited molecule. The presence of C_{60} has the effect of flipping the magnetization of some Cr atoms. In particular, Cr atoms surrounding the molecule have an opposite spin polarization with respect to those farther away from the vacancy. This observation finds an experimental evidence when comparing the XMCD spectra at the Cr $L_{2,3}$ edge of an uncovered Cr_4O_5/Fe(001) substrate (see Ref. 27) and of a 1 ML C_{60} covered Cr_4O_5/Fe(001) sample (see inset of Fig. 3b), as shown in Fig. 5g). In fact, the latter is clearly reduced by effect of the interaction with the C_{60} molecules, similarly to what has been reported for the XMCD signal at Fe $L_{2,3}$ edge in the C_{60}/Fe(001) case.[36]

In order to investigate how the fullerene molecule is affected by the magnetic properties of the surface layer, we analyzed the spin density ($\rho_{up} - \rho_{down}$) in the two energy ranges [0-1] eV and [2-3] eV from E_F, as shown in Fig. 5a-f), which show an opposite sign of the Cr_4O_5 magnetization, in agreement with Fig. 4. This property can be observed in Figs. 5e)
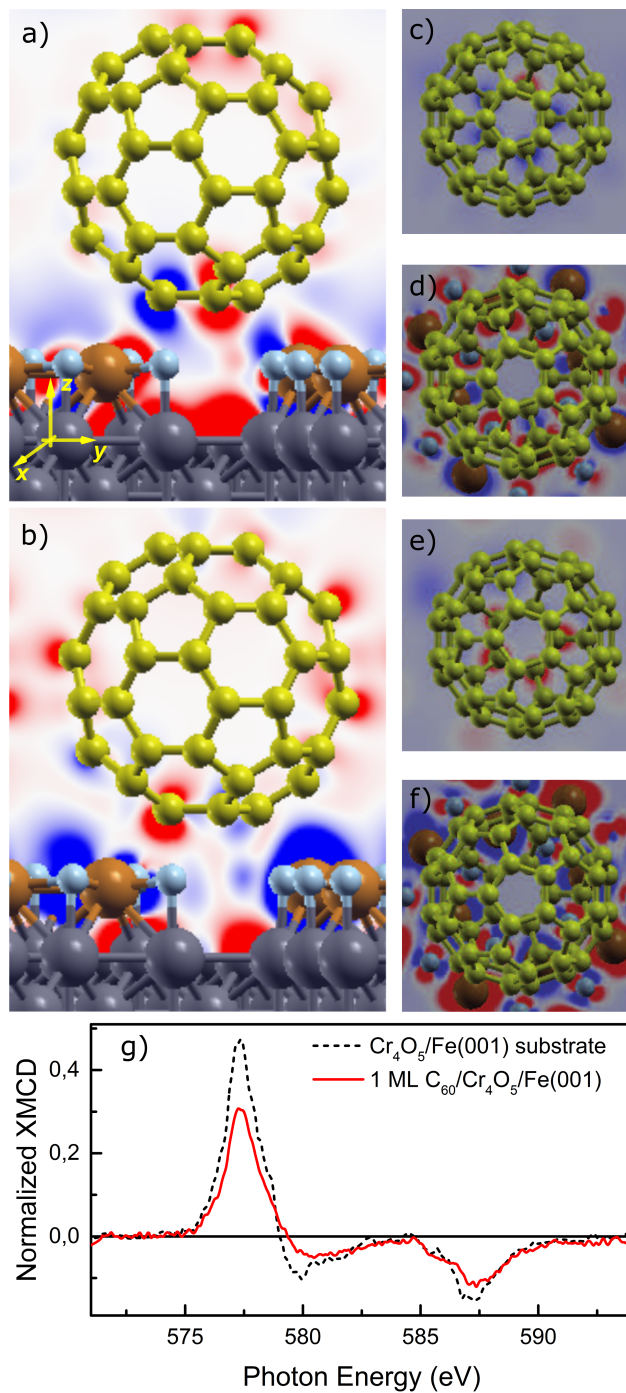
Figure 5: a), b) Section view of the spin density onto a (x, z) plane passing through the C atom with the core hole in the [0-1] and [2-3] energy ranges, respectively. c), d) The same as in a), b) but considering a (x, y) plane (i.e the plane parallel to the sample surface passing through the C atom with the core hole). e), f) The same as in c), d) for a (x, y) plane passing through the surface atoms. g) XMCD curves, calculated on normalized XAS spectra, of an uncovered $Cr_4O_5/Fe(001)$ substrate (black dashed line) and of a 1 ML C_{60} covered $Cr_4O_5/Fe(001)$ sample.

and 5f), which display a top view of the spin density on a (x, y) plane passing through the surface Cr_4O_5 layer in the two energy ranges. Figures 5a) and 5b) display a cut of the spin density in the (x, z) plane passing through the C atom with the core hole, in the same energy ranges. It shows that the molecule is indeed spin-polarized and that the magnetic character of the ionized atom is opposite to that of the substrate. Furthermore, the spin polarization of the molecule changes sign when changing energy range, as observed for the surface states. Similar observations can be made by inspecting Figs. 5c) and 5d), which shows cuts through the a (x, y) plane passing through the C atom with the core hole. These properties are in reasonable agreement with those observed in the XMCD spectra, which are characterized by the presence of peaks of opposite sign. The properties of the calculated spin densities confirm that, as discussed above, we can reasonably compare the XMCD signal relative to the other surfaces with the corresponding PDOS reported in Fig. 4, in agreement with the observation that the molecule spin polarization is an effect of the hybridization with the substrate.

In conclusion, we have discussed the properties of the interface between C_{60} and differently prepared Fe(001) surfaces: the pristine one, the oxygen-passivated Fe(001)-$p(1 \times 1)$O and the surface covered by a Cr_4O_5 wetting layer. The experimental results show that the insertion of a two-dimensional magnetic oxide directly influences both morphologic and electronic properties of the interface. Moreover, spin-polarized hybridized states were observed in all cases, with a particularly enhanced effect in the case of the C_{60}/Cr_4O_5 interface. Theoretical simulations supported the experimental results and emphasized the fact that tailoring the surface density of states of the substrate would allow to tailor the magnetic properties of a spinterface. Spinterfaces characterized by the presence of a two-dimensional magnetic oxide can thus be considered as reliable candidates for the design and development of organic spintronics systems.

References

(1) Xiong, Z. H.; Wu, D.; Vardeny, Z. V.; Shi, J. *Nature* **2004**, *427*, 821–824.

(2) Rocha, A. R.; García-suárez, V. M.; Bailey, S. W.; Lambert, C. J.; Ferrer, J.; Sanvito, S. *Nat. Mater.* **2005**, *4*, 335–339.

(3) Dediu, V. A.; Hueso, L. E.; Bergenti, I.; Taliani, C. *Nat. Mater.* **2009**, *8*, 707–16.

(4) Sun, D.; Ehrenfreund, E.; Valy Vardeny, Z. *Chem. Commun.* **2014**, *50*, 1781–1793.

(5) Zhang, X.; Mizukami, S.; Kubota, T.; Ma, Q.; Oogane, M.; Naganuma, H.; Ando, Y.; Miyazaki, T. *Nat. Commun.* **2013**, *4*, 1392.

(6) Wang, F.; Vardeny, Z. V. *Synth. Met.* **2010**, *160*, 210–215.

(7) Gobbi, M.; Golmar, F.; Llopis, R.; Casanova, F.; Hueso, L. E. *Adv. Mater.* **2011**, *23*, 1609–1613.

(8) Wong, P.; Tran, T.; Brinks, P.; van der Wiel, W.; Huijben, M.; de Jong, M. *Org. Electron.* **2013**, *14*, 451–456.

(9) Tran, T. L. A.; Le, T. Q.; Sanderink, J. G. M.; Van Der Wiel, W. G.; De Jong, M. P. *Adv. Funct. Mater.* **2012**, *22*, 1180–1189.

(10) Li, F.; Li, T.; Chen, F.; Zhang, F. *Org. Electron.* **2014**, *15*, 1657–1663.

(11) Liang, S.; Geng, R.; Yang, B.; Zhao, W.; Chandra Subedi, R.; Li, X.; Han, X.; Nguyen, T. D. *Sci. Rep.* **2016**, *6*, 19461.

(12) Zhang, X.; Ai, X.; Zhang, R.; Ma, Q.; Wang, Z.; Qin, G.; Wang, J.; Wang, S.; Suzuki, K.; Miyazaki, T.; Mizukami, S. *Carbon* **2016**, *106*, 202–207.

(13) Barraud, C.; Seneor, P.; Mattana, R.; Fusil, S.; Bouzehouane, K.; Deranlot, C.; Graziosi, P.; Hueso, L.; Bergenti, I.; Dediu, V.; Petroff, F.; Fert, A. *Nat. Phys.* **2010**, *6*, 615–620.

(14) Jiang, S. W.; Shu, D. J.; Lin, L.; Shi, Y. J.; Shi, J.; Ding, H. F.; Du, J.; Wang, M.; Wu, D. *New J. Phys.* **2014**, *16*, 013028.

(15) Schulz, L. et al. *Nat. Mater.* **2011**, *10*, 39–44.

(16) Ciudad, D.; Gobbi, M.; Kinane, C. J.; Eich, M.; Moodera, J. S.; Hueso, L. E. *Adv. Mater.* **2014**, *26*, 7561–7567.

(17) Zanettini, S.; Chaumy, G.; Chávez, P.; Leclerc, N.; Etrillard, C.; Leconte, B.; Chevrier, F.; Dayen, J.-F.; Doudin, B. *J. Phys.: Condens. Matter* **2015**, *27*, 462001.

(18) Li, D.; Barreteau, C.; Kawahara, S. L.; Lagoute, J.; Chacon, C.; Girard, Y.; Rousset, S.; Repain, V.; Smogunov, A. *Phys. Rev. B* **2016**, *93*, 085425.

(19) Shi, S.; Sun, Z.; Bedoya-Pinto, A.; Graziosi, P.; Li, X.; Liu, X.; Hueso, L.; Dediu, V. A.; Luo, Y.; Fahlman, M. *Adv. Funct. Mater.* **2014**, *24*, 4812–4821.

(20) De Jong, M. P. *Open Phys.* **2016**, *14*, 337–353.

(21) Cinchetti, M.; Dediu, V. A.; Hueso, L. E. *Nat. Mater.* **2017**, *16*, 507–515.

(22) Picone, A.; Riva, M.; Brambilla, A.; Calloni, A.; Bussetti, G.; Finazzi, M.; Ciccacci, F.; Duò, L. *Surf. Sci. Rep.* **2016**, *71*, 32 – 76.

(23) Zhan, Y. Q.; Liu, X. J.; Carlegrim, E.; Li, F. H.; Bergenti, I.; Graziosi, P.; Dediu, V.; Fahlman, M. *Appl. Phys. Lett.* **2009**, *94*, 1–4.

(24) Tran, T. L. A.; ÇakIr, D.; Wong, P. K. J.; Preobrajenski, A. B.; Brocks, G.; van der Wiel, W. G.; de Jong, M. P. *ACS Appl. Mater. Interfaces* **2013**, *5*, 837–841.

(25) Picone, A.; Giannotti, D.; Riva, M.; Calloni, A.; Bussetti, G.; Berti, G.; Duò, L.; Ciccacci, F.; Finazzi, M.; Brambilla, A. *ACS Appl. Mater. Interfaces* **2016**, *8*, 26418–26424.

(26) Picone, A.; Fratesi, G.; Riva, M.; Bussetti, G.; Calloni, A.; Brambilla, A.; Trioni, M.; Duò, L.; Ciccacci, F.; Finazzi, M. *Phys. Rev. B* **2013**, *87*, 085403.

(27) Brambilla, A.; Berti, G.; Calloni, A.; Picone, A.; Riva, M.; Bussetti, G.; Nappini, S.; Magnano, E.; Finazzi, M.; Duò, L.; Ciccacci, F. *J. Appl. Phys.* **2013**, *114*, 123905.

(28) Berti, G.; Calloni, A.; Brambilla, A.; Bussetti, G.; Duò, L.; Ciccacci, F. *Rev. Sci. Instrum.* **2014**, *85*, 073901.

(29) Bertacco, R.; Ciccacci, F. *Phys. Rev. B* **1999**, *59*, 4207–4210.

(30) Picone, A.; Brambilla, A.; Calloni, A.; Duò, L.; Finazzi, M.; Ciccacci, F. *Phys. Rev. B* **2011**, *83*, 235402.

(31) Jost, M. B.; Troullier, N.; Poirier, D. M.; Martins, J. L.; Weaver, J. H.; Chibante, L. P. F.; Smalley, R. E. *Phys. Rev. B* **1991**, *44*, 1966–1969.

(32) Brambilla, A.; Sessi, P.; Duò, L.; Finazzi, M.; Cabanillas-Gonzalez, J.; Egelhaaf, H.-J.; Lanzani, G.; Ciccacci, F. *Surf. Sci.* **2007**, *601*, 4078 – 4081.

(33) Panaccione, G. et al. *Rev. Sci. Instrum.* **2009**, *80*, 043105.

(34) Maxwell, A. J.; Brühwiler, P. A.; Arvanitis, D.; Hasselström, J.; Mårtensson, N. *Phys. Rev. Lett.* **1997**, *79*, 1567–1570.

(35) Maxwell, A. J.; Brühwiler, P. A.; Arvanitis, D.; Hasselström, J.; Johansson, M. K.-J.; Mårtensson, N. *Phys. Rev. B* **1998**, *57*, 7312–7326.

(36) Tran, T. L. A.; Wong, P. K. J.; De Jong, M. P.; Van Der Wiel, W. G.; Zhan, Y. Q.; Fahlman, M. *Appl. Phys. Lett.* **2011**, *98*, 222505.

(37) Wong, P. K. J.; Zhang, W.; Wang, K.; van der Laan, G.; Xu, Y.; van der Wiel, W. G.; de Jong, M. P. *J. Mater. Chem. C* **2013**, *1*, 1197.

(38) Donati, F.; Sessi, P.; Achilli, S.; Li Bassi, A.; Passoni, M.; Casari, C. S.; Bottani, C. E.; Brambilla, A.; Picone, A.; Finazzi, M.; Duò, L.; Trioni, M. I.; Ciccacci, F. *Phys. Rev. B* **2009**, *79*, 195430.

(39) Tange, A.; Gao, C. L.; Yavorsky, B. Y.; Maznichenko, I. V.; Etz, C.; Ernst, A.; Hergert, W.; Mertig, I.; Wulfhekel, W.; Kirschner, J. *Phys. Rev. B* **2010**, *81*, 195410.

(40) Weser, M.; Rehder, Y.; Horn, K.; Sicot, M.; Fonin, M.; Preobrajenski, A. B.; Voloshina, E. N.; Goering, E.; Dedkov, Y. S. *Appl. Phys. Lett.* **2010**, *96*, 012504.

(41) Perdew, J. P.; Burke, K.; Ernzerhof, M. *Phys. Rev. Lett.* **1996**, *77*, 3865–3868.

(42) Vanderbilt, D. *Phys. Rev. B* **1990**, *41*, 7892–7895.

(43) Giannozzi, P. et al. *J. Phys.: Condens. Matter* **2009**, *21*, 395502.

(44) Fratesi, G.; Lanzilotto, V.; Floreano, L.; Brivio, G. P. *J. Phys. Chem. C* **2013**, *117*, 6632.

(45) Monkhorst, H. J.; Pack, J. D. *Phys. Rev. B* **1976**, *13*, 5188–5192.